Available online at www.sciencedirect.com
SCIENCE DIRECT®
Journal of Catalysis 223 (2004) 36–43
JOURNAL OF CATALYSIS
www.elsevier.com/locate/jcat

Transient kinetics of carbon monoxide oxidation by oxygen over supported palladium/ceria/zirconia three-way catalysts in the absence and presence of water and carbon dioxide

R. Rajasree, J.H.B.J. Hoebink,* and J.C. Schouten

Laboratory of Chemical Reactor Engineering, Eindhoven University of Technology, P.O. Box 513, 5600 MB Eindhoven, The Netherlands

Received 19 August 2003; revised 15 December 2003; accepted 22 December 2003

Abstract

The transient kinetics of CO oxidation by O_2 over alumina-supported $Pd/CeO_2/ZrO_2$ three-way catalysts is described in the absence and presence of H_2O and CO_2 in the feed. Experiments were carried out in a laboratory fixed-bed reactor at 573 K, while periodically switching between a feed of 1 vol% CO in He and a feed of 0.5 vol% O_2 in He with a frequency of 1/30 Hz. Separate experiments were performed with 14 vol% water in both feeds, and, as is the case with real engine exhaust gas, with 14 vol% water and 14 vol% CO_2 in both feeds. The presence of water largely enhanced the reaction rate, while it was inhibited by CO_2. A transient kinetic model has been developed for this catalyst, based on the experimental data. It was found that the reaction in the absence of H_2O and CO_2 proceeds via the same elementary steps as reported for a $Pt/Rh/CeO_2/\gamma$-Al_2O_3 catalyst (R.H. Nibbelke, A.J.L. Nievergeld, J.H.B.J. Hoebink, G.B. Marin, Appl. Catal. B 19 (1998) 245). Only the rate coefficient for CO desorption from Pd was significantly lower, in line with literature data. Additional elementary steps were combined with the above model in order to describe quantitatively the effect of water. The present study also shows that bulk diffusion of oxygen in ceria plays a major role, when the rate is enhanced by water. The inhibition effect of CO_2 could be described by a lower amount of oxygen-storage sites.

Keywords: Kinetics; Modeling; Diffusion; CO oxidation; H_2O; CO_2; Three-way catalysis

1. Introduction

The use of three-way catalytic converters to reduce pollutants caused by automotive exhaust gases from Otto engines is well established and still provides the most efficient way. The three-way catalysts (TWC) simultaneously remove NO, CO, and hydrocarbons and consist of precious metals, promoters, and supports such as γ-Al_2O_3. Cerium oxide (CeO_2) has been proven to improve the thermal stability of the support, increase the noble metal dispersion, and act as oxygen-storage capacity (OSC) under oscillating conditions and is extensively added to the currently used three-way catalyst [2–5]. But it suffers from the drawback of thermal instability. In addition, OSC of the CeO_2 strongly decreases with thermal aging. Because of their superior aging stability and higher storage capability, mixtures of CeO_2 with oxides such as ZrO_2 are preferred nowadays over pure CeO_2 for TWC application [6,7].

Pd is the cheapest precious metal that is applicable in automobile converters. But Pt-loaded catalysts have been dominant for a long time because of their high tolerance against lead and sulfur poisoning. Due to a number of improvements in fuel quality, notably significantly lower lead and sulfur contents, and improved engine management systems, there is a growing demand for Pd-containing catalysts [8,9]. Therefore Pd-loaded ceria–zirconia mixed-oxide catalysts have been studied in this work.

The oxidation of CO and hydrocarbons and the reduction of nitrogen oxides over metals of a platinum group has been studied extensively both by experiments and by modeling during the past decades [10–13]. Transient kinetic studies of the individual reactions over a single catalyst were carried out recently [1,14–16]. Real engine exhaust gases, however, contain large amounts (10–14 vol%) of steam and carbon dioxide from the combustion processes taking place in the engine. Therefore, there is a signifi-

* Corresponding author.
E-mail address: j.h.b.j.hoebink@tue.nl (J.H.B.J. Hoebink).

0021-9517/$ – see front matter
doi:10.1016/j.jcat.2003.12.014

cant interest in the effect of these gases on catalyst performance.

It has been reported that water enhances the rate of reaction [17–22] and the presence of oxygen is required at temperatures too low for gas-phase water–gas-shift reactions to occur [21,22]. Furthermore, it is known that H_2O does not adsorb onto noble metal surfaces [23,24] but can adsorb on ceria [25] and alumina [26,27].

Hegedus et al. [17] and Muraki et al. [18] proposed that the presence of water would alter the CO oxidation equilibrium, but Campman [21] found evidence against this proposal. He performed a steady-state CO oxidation experiment using $H_2{}^{16}O$ and $^{18}O_2$ and discovered that conversion of CO to CO_2 occurs by the following reaction:

$$2C^{16}O + {}^{18}O_2 + 2H_2{}^{16}O \rightarrow 2C^{16}O_2 + 2H_2{}^{18}O.$$

This indicates that water is strongly involved in the oxidation of CO. A steady-state kinetic model involving monofunctional and bifunctional reaction paths was constructed by Nibbelke et al. [22] for CO oxidation by O_2 over $Pt/Rh/CeO_2/\gamma\text{-}Al_2O_3$ catalysts in the presence of 10 kPa H_2O and CO_2. The monofunctional path concerns the reaction between CO and O, both adsorbed on the noble metal. The bifunctional path involves CO on the noble metal and O from ceria. The accelerating effect of steam on the reaction is explained by an increased dissociation rate of molecular oxygen adsorbed on the ceria surface, with no net consumption of H_2O. The inhibiting effect of CO_2 on the reaction rate is explained by the adsorption of CO_2 on ceria, leading to the formation of carboxylate and carbonate species [28].

Harmsen [29] carried out experiments, where NO plus O_2 in He was alternated with C_2H_2, C_2H_4, and CO in He over $Pt/Rh/CeO_2/\gamma\text{-}Al_2O_3$ catalysts. The results were compared in a qualitative way with experimental results, where 10 vol% of H_2O and/or CO_2 was added to both reactor feeds. The findings show the enhancement of notably CO oxidation by water and inhibition by CO_2 as reported by Nibbelke et al. [22] and Li et al. [28]. The results also support that H_2O and CO_2 adsorb on ceria and not on noble metal [11, 30–32]. For quantitative modeling of the effect of H_2O and CO_2, Campman's proposal [21] did not work since the adsorption steps for oxygen, as directly taken from Nibbelke et al. [1], already assume instantaneous oxygen dissociation.

The objective of the present study is to investigate the applicability of the dynamic model developed by Nibbelke et al. [1] and to extend the model for CO oxidation by O_2 in the presence of H_2O and CO_2. The latter is not well understood from the viewpoint of elementary step kinetics and is important since oxygen storage on ceria is a dynamic process under automotive operating conditions. The model developed here is based on transient experiments at 573 K over Pd-loaded ceria–zirconia mixed-oxide catalysts, and can quantitatively describe the effect of H_2O and CO_2. The model developed by Nibbelke et al. [1] allows to predict the experimental data of the present study without involvement of H_2O and CO_2.

2. Experimental setup

The experimental setup, used for the present study, is described in detail elsewhere [21,33]. It consists of three sections: feed section, reactor section, and an on-line gas analysis section.

The feed section can generate two feed streams with different compositions. For each component, there is a blending system, which contains an electromagnetic valve and a thermal gas mass-flow controller. To add steam to both feeds, there are two HPLC pumps, which feed water into two evaporators. In order to prevent water condensation, all lines and devices downstream of the water evaporators are heated to 373 K. The two gas feed streams are alternated over the reactor by means of four magnetic valves. This is achieved by opening the valves two by two, in which one feed is passed to the reactor, while the other one is directed to the ventilation.

The reactor section consists of two tubular preheaters in parallel and a stainless-steel (type 316) fixed-bed reactor contained in an oven. The size of the catalyst bed is 15 mm length and 13 mm diameter. Actual switching between the feeds is achieved by sapphire bead valves, positioned downstream of the magnetic valves and preheaters near to the catalyst bed. This allows square-wave switches at high frequency [21,33]. Two infrared radiators placed inline with the reactor heat the reactor. Continuous sampling of inlet and outlet gas is carried out via capillaries, inserted immediately above and below the catalyst bed, and connected to the on-line mass spectrometer for real-time analysis. A high-resolution mass spectrometer (JEOL JMS-GCMate) was used for the analysis at a sampling frequency of 25 Hz [34].

The catalyst used is a Pd-loaded (2 wt%) ceria–zirconia mixed-oxide catalyst provided by the dmc^2 division of OMG, Hanau, Germany. The reactor contained typically 0.3 g of catalyst (0.11–0.15 mm pellet diameter), diluted with 0.47 g of inert $\alpha\text{-}Al_2O_3$ (diameter 0.15–0.21 mm) to establish a uniform catalyst bed temperature. The remaining reactor bed volume was filled with $\alpha\text{-}Al_2O_3$ to minimize dead volume as much as possible.

In order to obtain reproducible kinetic data, the catalyst, prior to experiments, was heated to 773 K in a flow of 5.6×10^{-3} mol s^{-1} He. Then, the catalyst was oxidized during 1 h by a stream containing 2 vol% of O_2 in He. Finally, the catalyst was allowed to cool down to reaction temperature under a helium stream of 5.6×10^{-3} mol s^{-1}.

3. Experimental results and discussion

The ranges of experimental conditions chosen in the present study are given in Table 1. Three types of cyclic feeding experiments have been carried out: (1) experiments with CO (1 vol%) in helium in one feed and oxygen (0.5 vol%) in helium in the other feed, (2) experiments same as type 1,

Table 1
Range of experimental conditions used for the development of the model

Temperature (K)	573
Total pressure (kPa)	110
Frequency (Hz)	1/30
p^0_{CO} (kPa)	0–1.0
$p^0_{O_2}$ (kPa)	0–1.0
$p^0_{H_2O}$ (kPa)	0–14.0
$p^0_{CO_2}$ (kPa)	0–14.0
W_{cat} (kg_{cat})	0.3×10^{-3}
Dilution ratio ($m^3_{inert}\, m^{-3}_{inert+cat}$)	0.48
Total flow (mol s^{-1})	5.6×10^{-3}
Duty cycle (%)	50

with 14 vol% water added to both feeds, and (3) experiments same as type 1, with 14 vol% of water and CO_2 in both feeds.

3.1. Experiments without H_2O and CO_2

Experiments without H_2O and CO_2 were carried out at 573 K, a switching frequency of 1/30 Hz, and a duty cycle of 50%. The feed stream containing CO (1 vol%) in He is alternated with O_2 (0.5 vol%) in He. The CO and O_2 concentrations in real time at the reactor outlet are given in Fig. 1A and for CO_2 in Fig. 1B. The first half-cycle shows the response after switching from O_2 to CO and the second one after switching from CO to O_2. The small CO_2 peak during the lean half-cycle concerns the transient oxidation of CO, adsorbed on the noble metal. This peak rapidly decays when the catalyst surface gets depleted from the nonfed reactant. The large CO_2 peak during the rich half-cycle results from two contributions. The maximum value refers mainly to the monofunctional path of reaction between CO and O on the noble metal. The tail of this peak deals with the bifunctional path, e.g., CO adsorbed on the noble metal and oxygen from the OSC. This is in accordance with previous work on CO oxidation by O_2 over $Pt/Rh/CeO_2/\gamma\text{-}Al_2O_3$ [1].

3.2. Experiments with H_2O

The experiments were carried out in a similar way as above, but with 14 vol% of water in both feeds. The CO and O_2 concentrations and the CO_2 concentration, all at the reactor outlet, are given in Figs. 2A and 2B, respectively. It is evident from the figures, when compared to Figs. 1A and 1B, that water enhances the rate of reaction on this catalyst as reported similarly in other studies for different catalysts [17–22]. The CO_2 peak maximum of both the rich and the lean half-cycle in Fig. 2B is slightly larger due to the presence of water than that observed in Fig. 1B. A similar rate enhancement was observed for $Pt/\gamma\text{-}Al_2O_3$ [22] and for $Pt/Rh/\gamma\text{-}Al_2O_3$ and $Rh/\gamma\text{-}Al_2O_3$ [21]. During the lean half-cycle, the CO_2 concentration decays rapidly, as was the case in the absence of water. An ongoing large production of CO_2 exists during the entire rich half-cycle, when only CO and not O_2 is fed to the reactor. This demands a continuous supply of oxygen from the OSC during the rich half-cycle, which apparently exceeds the amount of oxygen, available at the OSC surface, as the comparable signal in the absence of water (see Fig. 1B) decays much faster.

It is known that the oxygen atoms for the bifunctional reaction at the noble metal/oxide interface can be available by

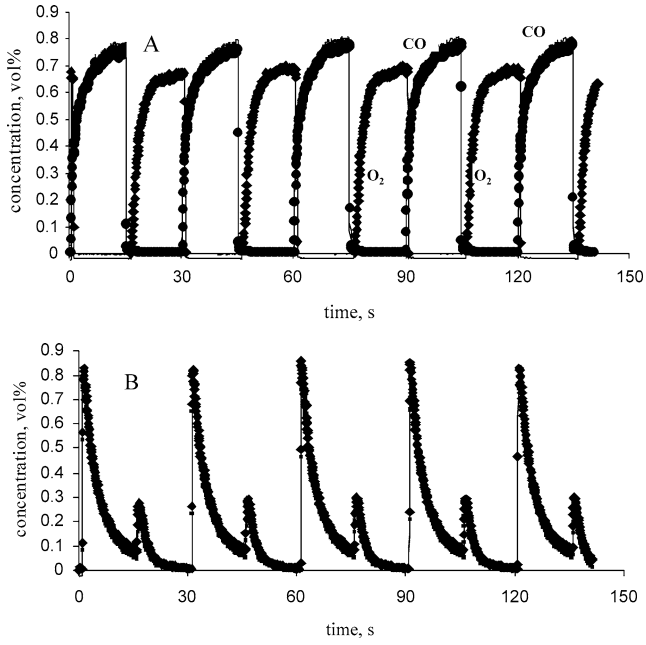

Fig. 1. Reactor outlet concentrations of CO and O_2 (A) and CO_2 (B) versus time. Markers, measured data points; curves, model predictions. Conditions: $T = 573$ K, frequency $= 1/30$ Hz, and in the absence of water.

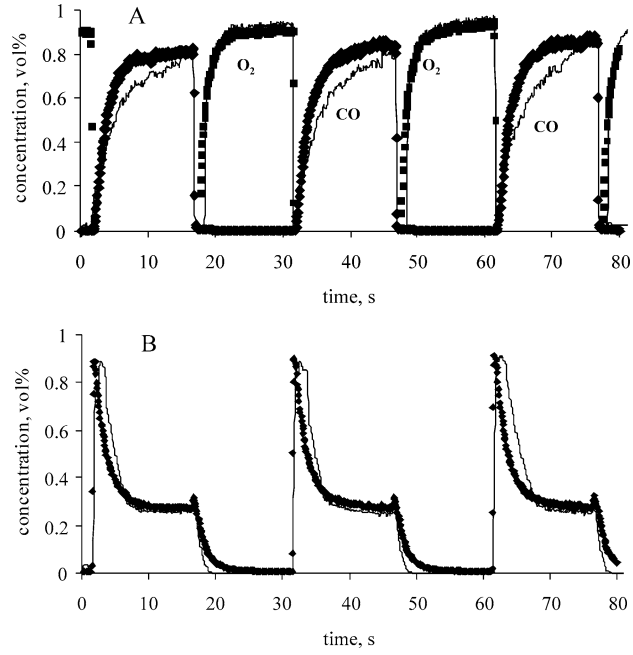

Fig. 2. Reactor outlet concentrations of CO and O_2 (A) and CO_2 (B) versus time. Markers, measured data points; curves, model predictions. Conditions: $T = 573$ K, frequency $= 1/30$ Hz, and in the presence of water.

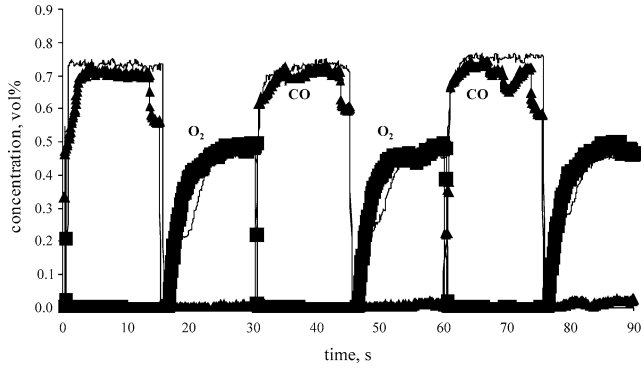

Fig. 3. Reactor outlet concentrations of CO and O_2 versus time. Markers, measured data points; curves, model predictions. Conditions: $T = 573$ K, frequency $= 1/30$ Hz, and in the presence of CO_2 and H_2O.

either surface diffusion of oxygen adsorbed on the OSC surface or by bulk diffusion of oxygen from the OSC lattice to the surface. Martin and Duprez [35] carried out diffusion studies and reported oxygen surface and bulk diffusion coefficients for various oxides. Nibbelke et al. [1] showed that bulk diffusion did not play a role in CO oxidation over Pt/Rh/CeO_2/γ-Al_2O_3, if water was absent. From the modeling studies, which will be discussed in the next section, the same appears for Pd-loaded ceria–zirconia mixed-oxide catalysts. In the presence of water, however, the diffusion of oxygen from the OSC bulk to surface is clearly involved in this particular case, even at 573 K.

3.3. Experiments with H_2O and CO_2

The experiments were carried out in a similar way as above, but with 14 vol% of CO_2 and 14 vol% of H_2O in both feeds. The CO and O_2 concentrations at the reactor outlet are given in Fig. 3. Due to the large amount of CO_2 in the feed, the CO_2 produced by CO oxidation is hard to distinguish from the signal's noise and is not shown here. The contribution of CO_2 mass fragmentation to the CO concentration was eliminated, but makes the CO signal less stable. It is evident from Fig. 3, that CO_2 inhibits the rate of reaction on this catalyst as found in other studies [28–32] with different catalysts. It has been reported that CO_2 does not adsorb on noble metal sites [11], but it can adsorb on ceria [28–32]. Also, CO_2 adsorption on ceria is reversible. Thus adsorption of CO_2 on ceria may lead to less vacant sites for oxygen adsorption and hence inhibits the rate of reaction.

4. Modeling results and discussion

A kinetic model for CO oxidation by O_2 over Pd-loaded ceria–zirconia mixed-oxide catalysts in the presence and absence of water and carbon dioxide has been developed in a similar way as described for CO oxidation by O_2 over Pt/Rh/CeO_2/γ-Al_2O_3 catalysts [1]. The aim of this modeling work is twofold: first, to test the applicability of the model developed by Nibbelke et al. [1], and second to construct the relevant elementary steps, which can predict quantitatively the influence of water and carbon dioxide.

The fixed-bed laboratory reactor used in this study is considered as an isothermal plug-flow reactor, with a constant molar flow rate along the catalyst bed. The model equations consist of four groups of continuity equations, namely gas-phase continuity equations (for CO, O_2, H_2O, and CO_2), surface species adsorbed on the noble metal surface, surface species adsorbed on the OSC surface, and CO_2 adsorbed on the support. A detailed description of the reactor model equations has been published [1]. In case H_2O is present, extra continuity equations are added for the relevant species, while an additional term is added to the continuity equation for O species on the OSC surface, describing diffusive transport between OSC bulk and surface (see Section 4.2).

To produce model predictions for reactor outlet concentrations, experimentally measured reactor inlet concentrations were used. The reactor inlet concentrations of H_2O and/or CO_2 present were set to zero when predicting the outlet concentrations in the absence of H_2O and CO_2, and kept at 14 vol% in the experiments with H_2O and CO_2 present. The rates of all elementary reaction steps were calculated via the law of mass action. Estimation of kinetic parameters, noble metal capacity, and oxygen-storage capacity of ceria–zirconia was obtained from nonlinear multiresponse regression analysis. The model calculations and regression analysis have been carried out in a similar way as reported earlier [1,29]. Since transient experiments provide data in a time-series format, individual data points cannot be considered as independent measurements, as would be the case for steady-state kinetic experiments. This makes an interpretation of the statistical significance rather complicated, notably for nonlinear systems, as has been discussed in detail [29].

4.1. CO oxidation by O_2 in the absence of H_2O and CO_2

To explore the applicability of the model developed by Nibbelke et al. [1] for CO oxidation by O_2 over Pt/Rh/CeO_2/γ-Al_2O_3 catalysts, the present study used exactly the same elementary reaction steps, which are shown in Table 2. The reaction mechanism consists of two monofunctional contributions (reaction paths A and B) and one bifunctional contribution (reaction path C). Reaction path A involves the competitive adsorption of CO and O_2 on the noble metal surface, followed by a Langmuir–Hinshelwood surface reaction. Reaction path B consists of CO adsorption on an oxygen atom, adsorbed on the noble metal surface, followed by reaction to CO_2. Reaction path C is the bifunctional reaction path, involving a reaction between CO adsorbed on the noble metal surface and oxygen from the ceria–zirconia surface.

The rate coefficients and the capacities (noble metal capacity and oxygen-storage capacity), as obtained by nonlinear multiresponse regression analysis of the CO, O_2, and CO_2 outlet concentrations, are presented in Table 3. The values reported by Nibbelke et al. [1], also given in Table 3,

Table 2
Elementary reaction steps [1] (for Pt/Rh/CeO_2/γ-Al_2O_3 catalyst), used in the kinetic modeling of the oxidation of CO by O_2 over a Pd-loaded ceria–zirconia-mixed-oxide catalyst in the absence of water and carbon monoxide

Step No.	Elementary reaction steps	Reaction path A σ_A	B σ_B	C σ_C
1	$CO + * \underset{k_1^b}{\overset{k_1^f}{\rightleftarrows}} CO*$	2	0	2
2	$O_2 + * \overset{k_2^f}{\rightarrow} O_2*$	1	1	0
3	$O_2* + * \overset{k_3^f}{\rightarrow} 2O*$	1	1	0
4	$CO* + O* \overset{k_4^f}{\rightarrow} CO_2 + 2*$	2	0	0
5	$CO + O* \underset{k_5^b}{\overset{k_5^f}{\rightleftarrows}} OCO*$	0	2	0
6	$OCO* \overset{k_6^f}{\rightarrow} CO_2 + *$	0	2	0
7	$O_2 + s \overset{k_7^f}{\rightarrow} O_2s$	0	0	1
8	$O_2s + s \overset{k_8^f}{\rightarrow} 2Os$	0	0	1
9	$CO* + Os \overset{k_9^f}{\rightarrow} CO_2 + * + s$	0	0	2
10	$CO_2 + \gamma \underset{k_{10}^b}{\overset{k_{10}^f}{\rightleftarrows}} CO_2\gamma$	0	0	0
	$2CO + O_2 \rightarrow 2CO_2$			

σ_i represents the stoichiometric number of the different reaction steps for reaction path i. $*$ denotes a noble metal site, s denotes a surface site of the oxygen-storage capacity, and γ denotes a support site.

Table 3
Kinetic parameters, noble metal capacity (L_{NM}), and oxygen storage capacity (L_{OSC}), obtained by regression of the cyclic feeding experiments at 573 K and a frequency of 1/30 Hz

Parameter	Units	Nibbelke et al. [1]	Present study: Without H_2O and CO_2	Present study: With H_2O or with H_2O and CO_2
k_1^f	$m^3\,mol^{-1}\,s^{-1}$	9.0×10^5	1.21×10^6	1.21×10^6
k_1^b	s^{-1}	125.74	3.24×10^{-3}	3.24×10^{-3}
k_2^f	$m^3\,mol^{-1}\,s^{-1}$	1.01×10^5	1.9×10^5	1.9×10^5
k_3^f	s^{-1}	∞	∞	∞
k_4^f	s^{-1}	25.13	1.012	1.012
k_5^b	s^{-1}	0.88	0.24	0.24
k_5^f	$m^3\,mol^{-1}\,s^{-1}$	4.72×10^3	2.88×10^3	2.69×10^3
k_6^f	s^{-1}	0.77	1.62	1.62
k_7^f	$m^3\,mol^{-1}\,s^{-1}$	11.36	0.23	2.46
k_8^f	s^{-1}	∞	∞	∞
k_9^f	s^{-1}	46.5	5.62	11.62
k_{10}^f	$m^3\,mol^{-1}\,s^{-1}$	10.1	11.62	1.883
k_{10}^b	s^{-1}	25.98	37.07	37.07
K_{11}^{eq}	$mol\,m^{-3}$	–	–	3.26×10^{-3}
K_{12}^{eq}	–	–	–	6.0×10^5
k_{13}^f	s^{-1}	–	–	2.68×10^{-3}
k_{14}^f	s^{-1}	–	–	20.9
D	$m^2\,s^{-1}$	–	–	6.0×10^{-14}
$L_{support}$	$mol\,kg_{cat}^{-1}$	0.15	0.15	0.15
L_{NM}	$mol\,kg_{cat}^{-1}$	0.15	0.2	0.2
L_{OSC}	$mol\,kg_{cat}^{-1}$	0.006	0.32	0.32 or 0.046[a]
ρ_p	$kg_{cat}\,m_p^{-3}$	2280	1580[b]	1580

The results are compared with the data of Nibbelke et al. [1], obtained by regression of cyclic feeding experiments at 393, 413, and 433 K.

[a] The value was 0.32 $mol\,kg_{cat}^{-1}$ if water only was present and 0.046 $mol\,kg_{cat}^{-1}$ with both H_2O and CO_2 present.

[b] Provided by OMG-dmc^2 division.

were used as initial guess values. The noble metal capacity of the current catalyst has the same order of magnitude as the catalyst of Nibbelke et al. [1]. The oxygen-storage capacity, however, appears to be a factor 50 larger. It should be expected that ceria/zirconia has a considerably larger storage capacity than ceria [36]. The support capacity was kept unchanged during the calculations, since the support is the same for both catalysts.

The calculated reactor outlet concentrations are presented, together with the experimental data, in Figs. 1A and 1B. There is a good agreement between measured and predicted data. Thus it can be concluded that the model developed by Nibbelke et al. [1] can be applied also for simulating the transient behavior over other three-way catalysts.

It is clear from Table 3 that the rates of adsorption of CO on noble metal (forward reaction in step 1), of adsorption of O_2 on noble metal (combined steps 2 and 3), of the reversible reaction between CO and oxygen adsorbed on noble metal (step 5), of the formation of CO_2 from $OCO*$ (step 6), and of the reversible adsorption of CO_2 on the support (step 10) have the same order of magnitude for the catalyst of Nibbelke et al. [1] and for the current catalyst. Differences can be explained on the basis of observed capacities, but in general the above coefficients are more or less the same for both catalysts.

The rate coefficient of CO desorption from the noble metal (backward reaction in step 1) is very low in the present study compared to the value reported by Nibbelke et al. [1]. This is notably due to the difference in the noble metal used, and such phenomenon has been observed by other researchers [37–39], where it is reported that desorption of CO from Pd is slowly occurring around 480 K, while CO desorption from Pt readily occurs at much lower temperatures. This slow rate of CO desorption from the noble metal has an effect on the surface reaction between CO and oxygen on noble metal (step 4), since a lower rate coefficient is found for the present catalyst.

It is also seen that the rate of adsorption of oxygen on oxide (step 7) has decreased considerably in the present study, which can be ascribed to the change in the oxygen-storage component. The change in the above rate parameter has an influence on the surface reaction between CO adsorbed on

the noble metal and oxygen adsorbed on the storage component (step 9), where there is a decrease in the rate coefficient with a factor of 10. This could be ascribed to a lower oxygen surface diffusivity for ceria/zirconia compared to ceria. Indeed Martin and Duprez [35] reported that at 673 K the oxygen diffusivity on the oxide surface of Rh/zirconia is a factor 100 smaller than for Rh/ceria. For Pt they were not able to measure the surface diffusivities, as the adsorption of oxygen became the rate-determining step.

4.2. CO oxidation by O_2 in the presence of H_2O

A kinetic model based on elementary steps was developed for the CO oxidation in the presence of 14 kPa water at 573 K. The elementary reaction steps considered for describing the effect of water are presented in Table 4. It is essentially a bifunctional reaction path involving CO adsorbed on noble metal and OH adsorbed on OSC.

In step 11, reversible adsorption of H_2O occurs on OSC sites forming H_2Os, which is assumed to be in equilibrium due to the high concentration of water. This step just explains the presence of adsorbed H_2O on the OSC. H_2Os reacts reversibly with oxygen on the OSC surface, forming adsorbed OH on OSC as presented in step 12. This OH group reacts with CO adsorbed on the noble metal, resulting in CO_2 and H adatoms, adsorbed on the OSC. The latter then react with OSC oxygen to form H_2Os, which closes the catalytic cycle.

It has been observed, when simulating the experimental data with the above steps incorporated in the mechanism of Table 2, that it was not possible to predict the experimental performance. A major discrepancy was that the amount of oxygen, consumed during the rich half-cycle by produced CO_2, was much higher than available from the noble metal surface and the OSC surface. Moreover the oxygen stored during the lean cycle exceeded considerably the surface capacities. Since the overall balances appeared to be closed, there is a strong suggestion that the OSC is larger by the involvement of bulk oxygen in ceria/zirconia. Therefore an oxygen diffusion flux was incorporated in the model. Apparently the rate enhancement of CO oxidation by the presence of water causes an early depletion of surface oxygen on the storage capacity during the rich half-cycle, as this oxygen is consumed via steps 9, 12, and 14. The surface oxygen depletion creates oxygen vacancies. Since there is no gaseous oxygen available to fill up these vacancies, diffusion of oxygen from bulk OSC to the surface takes place. This can also be represented as the diffusion of oxygen vacancies created at the oxide surface into the bulk of ceria. The opposite occurs during the lean half-cycle. Oxygen supply from the bulk explains the ongoing CO_2 production during the whole rich half-cycle.

Table 4
Elementary step reaction path considered for kinetic modeling of the effect of water on the oxidation of CO by O_2 over a Pd-loaded ceria–zirconia-mixed-oxide catalyst

Step No.	Elementary reaction steps	Reaction path, σ_D
1	$CO + * \underset{k_1^b}{\overset{k_1^f}{\rightleftarrows}} CO*$	2
7	$O_2 + s \overset{k_7^f}{\rightarrow} O_2s$	1
8	$O_2s + s \overset{k_8^f}{\rightarrow} 2Os$	0
11	$H_2O + s \underset{k_{11}^b}{\overset{k_{11}^f}{\rightleftarrows}} H_2Os$	0
12	$H_2Os + Os \underset{k_{12}^b}{\overset{k_{12}^f}{\rightleftarrows}} 2OHs$	1
13	$CO* + OHs \overset{k_{13}^f}{\rightarrow} CO_2 + Hs + *$	2
14	$2Hs + Os \overset{k_{14}^f}{\rightarrow} H_2Os + 2s$	1
	$2CO* + 2Os \rightarrow 2CO_2 + 2* + 2s$	

σ_D represents the stoichiometric number of the reaction steps for the extra reaction path D consisting of steps 12–14. Step 11 explains the presence of adsorbed H_2O. $*$ denotes a noble metal site, s denotes an oxygen storage capacity site. (Note that steps 1, 7, and 8 are the same as in Table 2.)

The flux of oxygen vacancies into the bulk of OSC is derived from the continuity equation for the oxygen vacancy fraction x_b in bulk OSC, assuming semi-infinite slab geometry. This assumption allows a rather simple relation for the flux through the outer surface of the OSC to be settled. It will hold if only a few layers underneath the outer surface take part in the process, which is the case when rich excursions do not last too long. Under the above assumption, Fick's second law for oxygen vacancy diffusion into the oxide is given by

$$\frac{\partial x_b}{\partial t} = D_0 \frac{\partial^2 x_b}{\partial r^2}, \tag{1}$$

where D_0 is the diffusivity of oxygen vacancies ($m^2\,s^{-1}$), r (m) is the distance from the surface, and x_b is the fraction of oxygen vacancies in the OSC bulk.

The initial condition at the start of the rich half-cycle is $t = 0$, $x_b = 0$.

The boundary conditions are:

$$t > 0, \quad r = 0 \text{ (at the surface)}, \quad x_b = x_s,$$

$$t > 0, \quad r = \infty \text{ (semi-infinite bulk)}, \quad x_b = 0,$$

with x_s the fraction of oxygen vacancies on the OSC surface. The flux ϕ_s through the interface surface is then given by

$$\phi_s = -N_s \rho_{cat} D_0 \left.\frac{\partial x_s}{\partial r}\right|_{r=0}, \tag{2}$$

with N_s the bulk concentration of vacancies (mol kg_{cat}^{-1}) and ρ_{cat} the catalyst density ($kg_{cat}\,m_{cat}^{-3}$). Solving Eqs. (1) and (2) with the boundary conditions leads to [40]

$$\phi_s = N_s \rho_{cat} \sqrt{D_0} \frac{1}{\sqrt{\pi}} \int_0^t \frac{1}{\sqrt{t-\tau}} \frac{\partial x_s}{\partial t}\, d\tau. \tag{3}$$

The integral in Eq. (3) can be solved numerically to provide

$$\phi_s^n = 2N_s\rho_{cat}\sqrt{D_0}\frac{1}{\sqrt{\pi}} \times \left[\sum_{k=0}^{n-1}\frac{x_{s,x}^{k+1}-x_{s,x}^{k}}{t^{k+1}-t^{k}}\left(\sqrt{t^n-t^k}\right)-\sqrt{t^n-t^{k+1}}\right], \quad (4)$$

with ϕ_s^n the flux at time t at axial position x of the reactor ($\mathrm{mol\,m^{-2}\,s^{-1}}$). The flux is positive when oxygen vacancies at the OSC surface diffuse into the bulk ceria, which means that at the same time oxygen from the bulk diffuses to the surface.

Regression analysis of the experimental data in the presence of water was carried out with the CO oxidation model (Table 2), including the water-enhancement effect (Table 4) and the oxygen-diffusion flux [Eq. (4)]. The capacities of noble metal, oxygen storage, and support were kept at the same values as in the case of no water in the feed. The reactor outlet concentrations, predicted by the model, are presented in Fig. 2A for CO and O_2, and in Fig. 2B for CO_2 along with the experimental data. It is seen that there is a good agreement between experimental and predicted values. The obtained rate parameters are given in Table 3 for comparison with the case without water.

The results for the reversible reactions 11 and 12 are reported as equilibrium coefficients, since simulations showed that an increase of the forward and backward rate coefficient with the same factor did not affect the model predictions. Apparently the rates of these steps are relatively large, which could be explained from the large excess of water. This also suggests that the majority of oxygen from the gas phase ends up in water, while water provides the oxygen for CO oxidation, as was observed by Campman [21] in his isotopic experiments.

It can be seen, when comparing columns 3 and 4 in Table 3, that almost all rate coefficients have the same or nearly the same values for the steps noted in Table 2, as should be expected. A notable difference is the adsorption of oxygen on the storage component, which is a factor of 10 larger for ceria/zirconia, because the rate enhancement by water causes a larger number of oxygen vacancies on the OSC surface.

The bulk diffusivity of oxygen vacancies was found to be $6\times10^{-14}\ \mathrm{m^2\,s^{-1}}$, which is much larger than the initial guess of $6\times10^{-22}\ \mathrm{m^2\,s^{-1}}$, as taken from the work of Martin and Duprez [35]. It should be noted, however, that the latter value was determined in the absence of water. It seems that water largely increases the mobility of oxygen in storage components.

4.3. CO oxidation by O_2 in the presence of H_2O and CO_2

The inhibiting effect of CO_2 on the reaction may be explained by the adsorption of CO_2 on ceria, leading to the formation of carboxylate and carbonate species. The above species can decrease the reaction rate of the bifunctional path (C and D) by decreasing the ceria surface available for oxygen adsorption. This in turn decreases the concentration of adsorbed oxygen on ceria and hinders the interface reaction, i.e., step 9 and step 13.

Hence the elementary steps considered in this case are the same as in the presence of water only. The rate coefficients and the capacities used to make model predictions are given in Table 3. The only difference between the cases of water only present and water and CO_2 present is in the oxygen-storage capacity (L_{osc}). The value of L_{osc}, when CO_2 and H_2O are present, is higher than in the absence of water and CO_2 and lower than in the presence of water only.

The predicted reactor outlet concentration for CO and O_2 is shown in Fig. 3. It is evident from Fig. 3 that there is a good agreement between the measured and the predicted data. As noted earlier, the high CO_2 feed concentration used in this case prohibits the successful measurement of CO_2 transients at the reactor outlet and is not interpreted.

5. Conclusions

The applicability of the dynamic model developed by Nibbelke et al. [1] is investigated for a different automotive catalyst and is extended for CO oxidation by O_2 in the presence of H_2O and CO_2. The study shows that this model can be applied for simulating the transient behavior over other three-way catalysts. Water enhances the rate of reaction and CO_2 inhibits the rate of reaction as reported in the literature. The effect of water is essentially a bifunctional reaction path involving CO adsorbed on the noble metal and OH adsorbed on the OSC. The bulk diffusion of oxygen in ceria plays a major role in the presence of water. The inhibition effect of CO_2 is described by a lower amount of oxygen-storage sites.

Acknowledgments

The authors gratefully acknowledge the dmc^2 division of OMG (Hanau, Germany) for providing the catalyst used in this study.

References

[1] R.H. Nibbelke, A.J.L. Nievergeld, J.H.B.J. Hoebink, G.B. Marin, Appl. Catal. B 19 (1998) 245.
[2] J.G. Nunen, H.J. Robota, M.J. Cohn, S.A. Bradley, J. Catal. 133 (1992) 309.
[3] M. Shelef, G.W. Graham, Catal. Rev.-Sci. Eng. 36 (1994) 433.
[4] R.W. McCabe, J.M. Kisenyi, Chem. Ind. 15 (1995) 605.
[5] A. Trovarelli, Catal. Rev.-Sci. Eng. 38 (1996) 439.
[6] P. Fornasiero, R. DiMonte, G. Ranga Rao, J. Kaspar, S. Meriani, A. Trovarelli, M. Graziani, J. Catal. 151 (1995) 68.
[7] G. Balducci, J. Kaspar, P. Fornasiero, M. Graziani, M.S. Islam, J. Phys. Chem. B 102 (1998) 557.
[8] S.K. Hoekman, Environ. Sci. Technol. 26 (1992) 1206.

[9] B.H. Engler, D. Lindner, E.S. Lox, S. Sindlinger, K. Ostgathe, Stud. Surf. Sci. Catal. 96 (1995) 441.
[10] N. Pacia, A. Cassuto, A. Pentenero, B. Weber, J. Catal. 41 (1976) 455.
[11] T. Engel, G. Ertl, Adv. Catal. 28 (1979) 1.
[12] R.K. Herz, S.P. Marin, J. Catal. 665 (1980) 281.
[13] P.J. Berowitz, C.H.F. Peden, D.W. Goodman, J. Chem. Phys. 92 (1988) 5213.
[14] J.M.A. Harmsen, J.H.B.J. Hoebink, J.C. Schouten, Ind. Eng. Chem. Res. 39 (2000) 599.
[15] J.M.A. Harmsen, J.H.B.J. Hoebink, J.C. Schouten, Chem. Eng. Sci. 56 (2001) 2019.
[16] J.M.A. Harmsen, J.H.B.J. Hoebink, J.C. Schouten, Catal. Lett. 71 (2001) 81.
[17] L.L. Hegedus, S.H. Oh, K. Baron, AIChE J. 23 (1977) 632.
[18] H. Muraki, S. Matunga, H. Shinjoh, M.S. Wainwright, D.L. Trimm, J. Chem. Technol. Biotechnol. 52 (1991) 415.
[19] J. Barbier, D. Duprez, Appl. Catal. B 4 (1994) 105.
[20] B.I. Whittington, C.J. Jiang, D.L. Trimm, Catal. Today 26 (1995) 41.
[21] M.A.J. Campman, Ph.D. thesis, Eindhoven University of Technology (1996).
[22] R.H. Nibbelke, M.A.J. Campman, J.H.B.J. Hoebink, G.B. Marin, J. Catal. 171 (1997) 358.
[23] J.M. Heras, L. Viscido, Catal. Rev.-Sci. Eng. 30 (1988) 281.
[24] Y.K. Peng, P.T. Dawson, Can. J. Chem. Eng. 55 (1979) 1658.
[25] C. Padeste, N.W. Cant, D.L. Trimm, Catal. Lett. 18 (1993) 305.
[26] E.C. DeCanio, J.C. Edwards, J.W. Brudo, J. Catal. 148 (1994) 76.
[27] H. Cardona-Martinez, J.A. Dumesis, Adv. Catal. 38 (1992) 149.
[28] C. Li, S. Yoshihisa, A. Totu, D. Kazunari, M. Ken-ichi, O. Takaharu, J. Chem. Soc., Faraday Trans. 85 (1989) 1451.
[29] J.M.A. Harmsen, Ph.D. thesis, Eindhoven University of Technology (2001).
[30] R.K. Herz, Ind. Eng. Chem. Prod. Res. Dev. 20 (1981) 451.
[31] T. Jin, T. Okuhara, G.J. Mains, J.M. White, J. Phys. Chem. 91 (1987) 3310.
[32] C. Li, Y. Sakata, T. Arai, K. Domen, K. Maruya, T. Onshi, J. Chem. Soc., Faraday Trans. 85 (1989) 929.
[33] J.H.B.J. Hoebink, A.J.L. Nievergeld, G.B. Marin, Chem. Eng. Sci. 54 (1999) 4459.
[34] J.M.A. Harmsen, Th. Bijvoets, J.H.B.J. Hoebink, T. Hachiya, J. Bassett, A.D. Brooker, J.C. Schouten, Rapid Commun. Mass Spectrometry 16 (2002) 957.
[35] M. Martin, D. Duprez, J. Phys. Chem. 100 (1996) 9429.
[36] M.H. Yao, R.J. Baird, F.W. Kunz, T.E. Hoost, J. Catal. 166 (1997) 67.
[37] J.A. Rodriguez, Surf. Sci. 345 (1996) 347.
[38] A. Ortega, F.M. Hoffman, A.W. Bradshaw, Surf. Sci. 119 (1982) 79.
[39] M.P. Kiskinova, G.M. Bliznakov, Surf. Sci. 123 (1982) 61.
[40] R.H. Nibbelke, J. Scheerova, M.H.J.M. De Croon, G.B. Marin, J. Catal. 156 (1995) 106.